Subnanosecond transient-reflecting-grating measurements and depth-profiling analysis of mesoscopic subsurface properties of a nickel single crystal

Akira Harata
Department of Molecular and Material Sciences, Graduate School of Engineering Sciences, Kyushu University, 6-1 Kasugakoen, Kasuga-shi, Fukuoka, 816-8580, Japan

Naoyasu Adachi and Tsuguo Sawada
Department of Applied Chemistry, School of Engineering, The University of Tokyo, 7-3-1 Hongo, Bunkyo-ku, Tokyo 113-8656, Japan
(Received 24 March 1998)

Subnanosecond transient reflecting grating measurements were made for a mirror-polished (110) surface of a Ni single crystal under temperature control from 93–273 K and with a variety of grating spacings from 1–4 μm. The experimental responses were compared with theoretically calculated ones. Agreement was good for large grating spacings and at room temperature, but larger deviations appeared as temperature was lower or grating spacing was made smaller. The results suggested that the mesoscopic subsurface region of a submicrometer size had a different thermal diffusivity from the bulk material. The measured responses were analyzed to deduce temperature dependence of thermal diffusivity as well as acoustic velocity in the subsurface region. A depth profiling analysis of the thermal diffusivity was carried out to allow discussion of mechanisms of the diffusivity decrease. [S0163-1829(98)00836-4]

I. INTRODUCTION

Photothermal and photoacoustic (PT/PA) phenomena have been widely applied to determine thermal and elastic properties of materials as well as to measure absorption spectra and to detect ultratrace compounds.[1,2] Both homogeneous and inhomogeneous material systems are welcome targets. Above all, the PT/PA measurements are powerful tools for the latter systems because of their own potentiality for nondestructive depth profiling analysis of opaque materials and of their own remote sensing capability. It is easily understandable for an opaque material illuminated by a pulsed light generating heat just at the surface that higher time-resolved PT/PA measurements provide material properties of a shallower surface region. This is because heat diffuses over a finite distance in a given time interval. Recently, fast and ultrafast PT/PA phenomena have become observable by using laser-based optical techniques.[3] With ps temporal resolution, a region just tens of nanometers form a surface (mesoscopic subsurface) of a metal becomes accessible so that surface-specific transport property can be investigated. It is well known that a metal surface exhibits specific electrical conductivity due to electron scattering by the surface itself[4] and surface-specific structures. Since thermal conduction in a metal is dominated by electron transport,[5] thermal conductivity near the surface should be influenced by electron scattering by that surface. Additional influences on heat conduction can be produced by lattice damages localized near the surface, which are introduced during surface processing procedures, as a matter of course, even for silicon wafers fabricated by well-established techniques.[6]

A subnanosecond time-resolved transient reflecting grating (TRG) is one ultrafast optical technique for measuring fast PT/PA phenomena occurring at the subsurface or interface of opaque materials.[3] A transient grating is formed when two coherent optical pulses (excitation pulses) cross in or on a material.[7] For a metal, the transient grating is generated only near the surface and it is observable as a TRG by detecting the reflecting diffraction of another laser beam (probe beam) from the transient grating on the surface.[8] The TRG signals are sensitive and selective to the surface or interface,[9–11] where the experimentally controllable condition of grating spacing is a measure of observation depth under the surface. Since the relaxation dynamics of the TRG reflects optical, thermal, and acoustic properties of the material, these properties can be quantitatively determined for the selected observation depth. Transient response of TRG signals have been compared with analytical theory,[12] or been analyzed with an empirical equation to deduce surface-specific material properties.[13]

In this paper, subnanosecond TRG measurements were carried out for a mirror-polished (110) surface of a Ni single crystal under temperature control from 93–273 K and with a variety of grating spacings from 1–4 μm. The measured responses were compared with theoretical calculations. We found good agreement between measured and calculated responses at room temperature and with large grating spacings, but there were substantial deviations at low temperatures or small grating spacings. The observation corresponded to a decrease of thermal diffusivity in the mesoscopic subsurface. The measured TRG responses were analyzed to deduce thermal diffusivity and velocity of surface acoustic waves (SAW) by using a fitting procedure with the empirical equation. A depth profiling analysis of the thermal diffusivity was carried out to allow us to discuss mechanisms of the diffusivity decrease in the mesoscopic subsurface.

In Sec. II, we explain our experimental setup and procedures for data analysis. Section III describes the theory we use, in which an isotropic and homogeneous metal is assumed to solve coupled equations of heat diffusion and elastic wave propagation after pulsed and holographic light illumination. We relate the theory to the empirical equation used

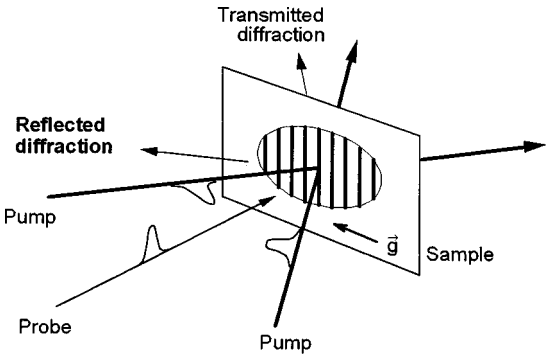

FIG. 1. Two crossing laser pulses excite a transient grating at the crossing point, which is detectable as a transient reflecting grating.

to analyze the TRG responses of a real sample. In Sec. IV, we compare measured and calculated results and discuss dependence on temperature and grating spacings and a depth profiling analysis. Section V summarizes the conclusions reached in the present work.

II. EXPERIMENT

A. Measurement of TRG responses

Two temporally coincident laser pulses (pump pulses), having the same wavelength and polarization, interfere with each other to form a transient holographic pattern at their crossing point. When we set an opaque sample at the crossing point, the sample surface is illuminated by the interference fringes. The illumination makes the surface temporally behave like a diffraction grating as shown in Fig. 1. A third laser pulse (probe pulse) will be diffracted off, if its incident has an appropriate timing with respect to the pump pulses.

When the pump pulses have incident angles of θ and $-\theta$, respectively, so as to have a crossing angle of 2θ, the interference fringes have a spacing of Λ equal to $\lambda/2 \sin\theta$ where λ is the pump light wavelength.[7] It is experimentally important that Λ is controllable by changing θ. Another point is that detection of diffraction in reflection is not only suitable for surface selective observation,[9] but also essential for investigating nontransparent materials such as metals. The pump-and-probe technique is often adopted for fast and ultrafast investigation as in the present study.

With the experimental setup shown in Fig. 2, using a subnanosecond laser, we can observe fast heat transport at the surface and GHz-SAW as shown in Fig. 3. Optical excitation of the metal surface by the optical fringes results in formation of the same sinusoidal patterns of temperature, acoustic strain, and so on. These patterns locally exist only near the surface to work as a TRG. Formation and decay of the TRG carry information on material properties within a restricted region near the surface, i.e., a subsurface.

A mode-locked Q-switched Nd:YAG (yttrium aluminum garnet) laser (Quantronix, model 416) was operated with a single pulse selector and a potassium titanyl phosphate (KTP) doubling crystal. The output pulse had an 80 ps duration, 532 nm wavelength, and 1.13 kHz repetition. A single pulse was divided into three. Two of them, having an equal intensity, excited the TRG in the 60 μm spot and the third pulse, with a weaker intensity, was used as a probe. Their

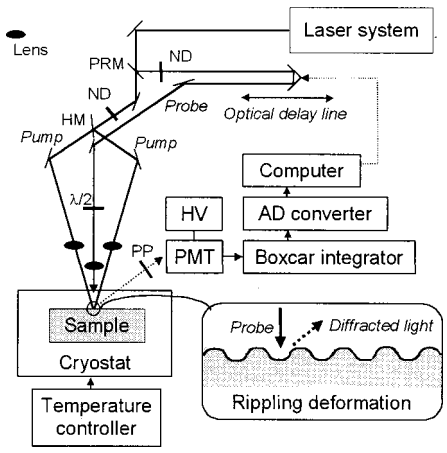

FIG. 2. Experimental setup of the TRG measurement. (HM), half mirror; (HV), high voltage power supply; (ND), neutral density filter; (PMT), photomultiplier tube; (PRM), partly reflective mirror; (PP), polarizer; ($\lambda/2$), half-wave plate; and the other optical elements are mirrors.

intensities were adjusted to less than 100 nJ for each pump pulse and 10 nJ for the probe pulse with two neutral density filters set to prevent the sample surface from damage. The probe pulse passed though an optical delay line and was normally irradiated onto the TRG. Diffracted light was detected with a photomultiplier tube (PMT) whose entrance was placed at the position of one of the first order diffraction spots. The output signal from the PMT was gated and averaged over 1 ms with a boxcar integrator connected to an analog to digital converter. A TRG response was obtained on a computer by recording the signal intensity as a function of the delay time of the probe pulse. The maximum time window of observation was limited to 13.3 ns by the 4 m length of the optical delay line. Each response, with a 12.8 ns window, consisted of 512 data points of the same time interval.

The sample to be used was cut parallel to a (110) face from a single crystalline Ni stick of 99.99% purity grade.

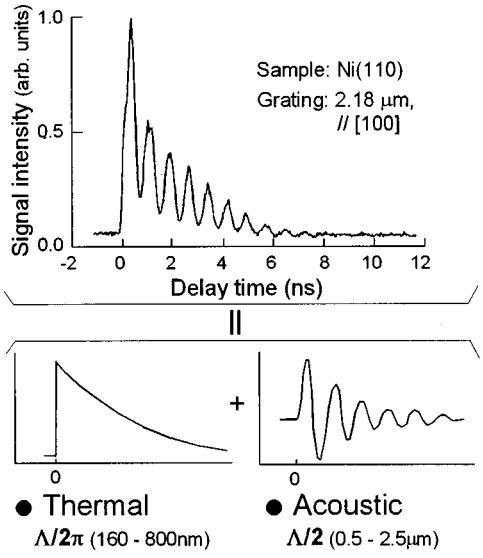

FIG. 3. Typical TRG response of the Ni single crystal. A TRG response is considered as a superposition of thermal and acoustic contributions. Observation depth for each contribution is indicated at the bottom for grating spacing Λ of 1 to 5 μm.

The sample surface, with an area of 10 mm×10 mm, was carefully mirror-polished with ultrafine alumina powders. The sample was cleaned and rinsed with methanol and dried before being placed in a cryostat having an optical window (80 mm diameter). The cryostat could be evacuated by a rotary pump. The sample temperature was controlled with a better precision than ±2 K at every temperature ranging from 80–297 K.

TRG measurements were done for a variety of conditions: (a) at room temperature with grating spacings varied from 1.05–3.59 μm, and (b) with a fixed grating spacing of 1.84 μm under temperature control both in a cooling cycle at 273, 243, 213, 183, 153, 123, and 93 K and in a heating cycle at 123, 173, 223, and 273 K of the sample. For each grating spacing in measurement (a), more than 16 responses were measured and separately analyzed in the way described below to get averaged values and standard deviations of characteristic parameters describing the transient wave forms. For each temperature in measurement (b), more than 14 responses were measured at each temperature in the cooling cycle, and four responses were measured at each temperature during the heating cycle. In all measurements, the grating vector was set parallel to the [100] direction of the Ni crystal.

B. Analysis of transient wave forms with an empirical equation

An empirical formula representing the TRG response was used for data analysis to deduce some characteristic material properties. It is given by[3]

$$S_{\mathrm{TRG}}(t)=R_P I_P I_0^2 A^2[\exp(-t/\tau_T) - r\ \exp(-t/\tau_A)\cos\{2\pi F(t+t_D)\}]^2, \qquad (1)$$

where R_P is reflectivity for the probe light and I_P and I_0 are probe and pump light intensities, respectively. This empirical equation represents $S_{\mathrm{TRG}}(t)$ as being proportional to the square of a grating amplitude that is given as a linear combination of thermal and acoustic components. The equation contains six adjustable parameters. The meaning of each parameter is as follows: A is an intensity factor depending on the amount of absorbed pump energy, etc.; τ_T, a thermal relaxation time constant; r, a coupling constant between the slowly decaying and oscillating components; τ_A, SAW attenuation constant; F, SAW frequency; and t_D, delay time in SAW generation. These six parameters can be uniquely defined for a given TRG response because their correlation is not so close. Good fitting results have been gotten for various materials, which provide local material properties quantitatively.[13,14]

We determined the thermal relaxation time constant τ_T and SAW frequency F for each of the TRG responses measured under the various experimental conditions. We used a nonlinear least square method to fit the measured response $S_{\mathrm{measured}}(t)$ to Eq. (1). The fitting procedure was as follows: First, baseline level S_{BG} was determined from data points of negative delay time. After it was subtracted from the response, square roots were calculated as $\sqrt{S_{\mathrm{measured}}(t)-S_{BG}}$, from which an oscillation frequency F was roughly estimated using fast Fourier transform. The square rooted response was smoothed over a time-interval $1/F$ to eliminate the oscillation. From the smoothed response, we estimated an exponential decay constant $1/\tau_T$ and a preexponential factor A. From subtraction of the $\sqrt{S_{\mathrm{measured}}(t)-S_{BG}}$ and its smoothed response, r, τ_A, and t_D were estimated. Setting these roughly estimated parameters as initial values, we minimized the summation of squared errors between $S_{\mathrm{measured}}(t)-S_{BG}$ and Eq. (1) by a step-by-step calculation during slight parameter changes. In the calculation, we used more than 300 data points corresponding to delay times over 0.5 ns after the TRG signal was its maximum. After the calculation for each response, averaged values and standard deviations were obtained for $1/\tau_T$ and F for each measurement condition.

C. Estimation of thermal diffusivity and SAW velocity, and their observation depths

The relation $1/\tau_T=1/\tau_0+D(2\pi/\Lambda)^2$ approximately holds where D is thermal diffusivity for surface-parallel heat transport and τ_0 is a constant representing surface-normal heat transport.[3,15] For an inhomogeneous system such as a layer system, D represents an effective thermal diffusivity D_{eff}. It means an averaged diffusivity from the top surface to a depth Λ/π. Since we cannot determine D_{eff} and $1/\tau_0$ at the same time for a fixed grating spacing measurement, a further approximation neglecting $1/\tau_0$ is used in Sec. IV B, namely,

$$D_{\mathrm{eff}}=\Lambda^2/4\pi^2\tau_T. \qquad (2)$$

It is important to note that D_{eff} is likely to be overestimated since this treatment means we ignore heat diffusion into the depth direction. SAW velocity V_{SAW} was calculated as a product $F\Lambda$. For a homogeneous isotropic material surface, the SAW is in a Rayleigh mode[8,12] so that its energy is localized within one acoustic wavelength from the surface.[16]

In the present TRG measurements, light is absorbed near the sample surface and heat is generated there. The heat diffuses near the surface and the SAW propagates along the surface. Thus, all of the optical, thermal, and elastic energies causing the TRG signal are localized near the surface. As indicated above, we can estimate observation depth, which is a quantitative measure showing where we observe under the surface. Here we use as observation depths $\Lambda/2\pi$ and $\Lambda/2$ for thermal and elastic properties, respectively. Roughly, they indicate the centers of thermal or acoustic energy.

III. THEORY

Theoretical treatments of TRG as well as the transient grating have been reported in several studies.[17–19] However, some of them neglect heat diffusion, and the others are in somewhat complicated forms to describe multilayer systems. Here we take a simple form describing the TRG response for a homogeneous and isotropic solid surface within the limit of a weak perturbation. Our purpose is to acquire a good insight into measured responses for analysis and depth profiling.

A. Formation of a transient grating on a metal surface

When a crystalline metal is illuminated by an intense laser beam, anisotropic or nonlinear electronic or thermal effects arise. However, for simplicity, we neglect anisotropic heat diffusion and assume magnitudes of temperature rise Φ and

displacements **U** induced by laser illumination are small enough to be treated with linear expressions. Two elastic constants are equivalently deduced for a certain direction of acoustic propagation from three elastic constants of the cubic crystal.

The model treated here is as follows. When the pump pulses produce the transient holographic pattern on the metallic surface at $z=0$ in the xy-plane, Φ and **U** made from heat generation succeeded by thermal expansion in the material are governed[20] by equations,

$$\frac{\partial \Phi}{\partial t} = D\nabla^2\Phi + \frac{2I_0(1-R)\beta}{\rho C_P}\exp(-\beta z)(1+\cos\Delta y)g(t), \tag{3}$$

$$\frac{\partial \mathbf{U}}{\partial t} = \frac{E}{2\rho(1+\nu)}\nabla^2\mathbf{U} + \frac{E}{2\rho(1+\nu)(1-2\nu)} \times \nabla(\nabla\cdot\mathbf{U}) - \frac{E\alpha\nabla\Phi}{2\rho(1-2\nu)}, \tag{4}$$

where D is thermal diffusivity ($=\kappa/\rho C_P$, κ is thermal conductivity; ρ is density; C_P is heat capacity), I_0 is the time-averaged light energy density, R is the undisturbed reflectivity, and β is the effective absorption coefficient that is slightly dependent on the incident angle.[21] Δ is the wave number of the interference fringes given by $\Delta=2\pi/\Lambda$, where Λ is the grating spacing and it is equal to the SAW wavelength.[7,10] $g(t)$ represents temporal profile of the light pulse. E is Young's modulus, ν is the Poisson ratio, and α is the linear thermal expansion coefficient. In Eq. (3), we neglect a coupling term between Φ and **U** because our experimental condition was within the limit of an acoustic frequency of less than 10 GHz and small displacement.[20] For boundary conditions to be satisfied, we neglect heat flux and use force valance at $z=0$. At first, we assume $g(t)$ being the delta function and instantaneous heat generation just after the light illumination. Although it takes a few picoseconds for photoexcited electrons in a metal to diffuse and relax to the local thermal equilibrium of the electron and lattice,[22] the time is short enough for our experiment.

In the transient grating experiment, only the spatially modulated terms in the y direction are important. When the spatially nonmodulated parts are ignored, linearity and spatial symmetry of the problem require that the temperature rise Φ and displacements **U** are represented as $\varphi(z,t)\cos(\Delta y)$ and $\mathbf{e}_Y u_Y(z,t)\sin(\Delta y)+\mathbf{e}_Z u_Z(z,t)\cos(\Delta y)$, respectively, where $\mathbf{e}_Y$ and $\mathbf{e}_Z$ are unit vectors of the system and $\mathbf{e}_Y$ is parallel to the grating wave vector and $\mathbf{e}_Z$ is perpendicular to the surface. Laplace transform in time provides a set of analytically solvable differential equations with respect to z. The solutions for $z=0$ have simple forms given by

$$\hat{\varphi}(0,s) = \frac{2I_0(1-R)}{\kappa\Delta}\frac{\gamma_1}{\gamma_2(\gamma_1+\gamma_2)}, \tag{5a}$$

$$\hat{u}_Y(0,s) = -\frac{2\gamma_4}{\gamma_4^2+1}\hat{u}_Z(0,s), \tag{5b}$$

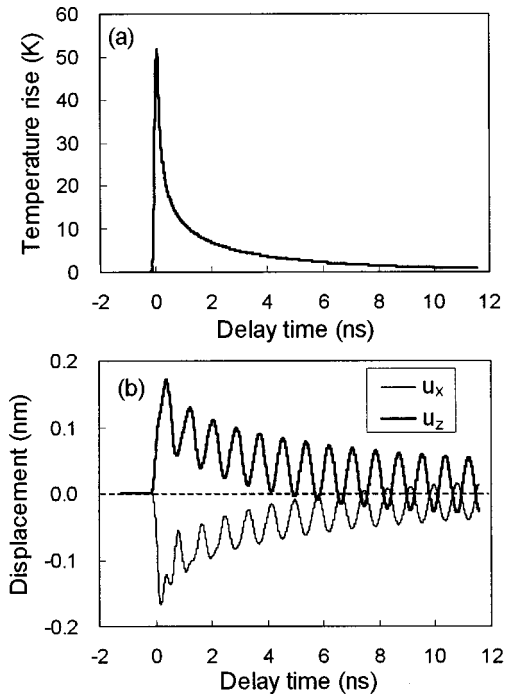

FIG. 4. Calculated responses for the Ni single crystal: Amplitudes of surface-parallel spatial modulation in (a) temperature; (b) displacement to surface-parallel (u_x) and surface-normal (u_z) direction. The grating spacing is 2.5 μm.

$$\hat{u}_Z(0,s) = -\frac{2I_0(1-R)\alpha(1+\nu)}{\kappa\Delta^2(1-\nu)}\frac{\gamma_1}{\gamma_2(\gamma_1+\gamma_2)} \times \frac{\gamma_1+\gamma_2+\gamma_3}{(\gamma_2+\gamma_3)(\gamma_3+\gamma_1)}\frac{\gamma_4^4-1}{(1+\gamma_4^2)^2-4\gamma_3\gamma_4}, \tag{5c}$$

where $\hat{\varphi}$, $\hat{u}_Y$ and $\hat{u}_Z$ are Laplace transforms of φ, u_Y, and u_Z, respectively. γ_i ($i=1,2,3,4$) are given by $\gamma_1=\beta/\Delta$, $\gamma_2=(1+s/\Delta^2 D)^{1/2}$, $\gamma_3=(1+s^2/\Delta^2 V_L^2)^{1/2}$, and $\gamma_4=(1+s^2/\Delta^2 V_T^2)^{1/2}$ where $\mathrm{Re}\{\gamma_i\}\geqslant 0$, and V_L and V_T are longitudinal and shear acoustic velocities, respectively. Inversion of the Laplace transform is given by the Bromwich integral

$$f(t) = \frac{1}{2\pi j}\int_{r-j\infty}^{r+j\infty}\hat{f}(s)\exp(st)ds, \tag{6}$$

which provides values of $\varphi(z,t)$, $u_Y(z,t)$, and $u_Z(z,t)$. We numerically calculated inversion of the Laplace transform based on an integration method, where the exponential term in Eq. (6) was replaced by a well-characterized function.[23–25] The replacement provides a good result for the integral by taking a partial summation of its kernel before adding some compensation terms using the fifth Euler's transformations.

Figure 4 represents calculated results of $\varphi(0,t)$, $u_Y(0,t)$, and $u_Z(0,t)$ for grating spacing of 2.5 μm. We took temporal profile of the pump beams into account by calculating their convolution integrals with a Gaussian-type function $g(t)=(\sqrt{2/\pi}/\tau_p)\exp[-2(t/\tau_p)^2]$, where τ_p is a measure of the pulse width. Responses of the surface displacements shown in Fig. 4(b) have similar shapes to those calculated for a n-TiO_2 crystal by Faran, Miller, and Gracewski,[26] except for

slowly decaying features representing thermal diffusion effects, which were neglected in their work.

B. Transient reflecting grating response

Light diffraction from a TRG on a metal surface is mainly caused by surface-normal deformation with a minor effect from reflectivity modulation induced by the temperature distribution. For the Ni sample, we assume TRG signal $S_{\mathrm{TRG}}(t)$ is quadratically proportional to $u_Z(0,t)$ as

$$S_{\mathrm{TRG}}(t)=K[u_Z(0,t)]^2 \tag{7}$$

where K is a time-independent constant, which can be estimated[13] for a given experimental condition with literature values of material optical properties.[27] It may be possible for the probe light penetrating into the metal to have some influence on light diffraction because there is a photo-induced refractive index variation under the metal surface. However, since the biggest change in the refractive index is at the surface, where direction of light propagation has the largest influence, the refractive index modulation just at the surface might cause the biggest influence on the TRG signal. This means the $\varphi(0,t)$ term could couple to $S_{\mathrm{TRG}}(t)$. Although such coupling has been observed for a gold film under a plasmon resonance condition,[28] we conclude that this coupling is negligible for Ni when the probe beam almost normally illuminates the sample. To evaluate $S_{\mathrm{TRG}}(t)$ theoretically, we took into account the temporal profile $g(t)$ for the probe beam as convolutions of $g(t)$ with Eq. (7). We make a comparison of the calculated $S_{\mathrm{TRG}}(t)$ with the experimental $S_{\mathrm{measured}}(t)-S_{BG}$ in Sec. IV A.

C. Consideration on the surface-normal displacement response for depth profiling analysis

Up to now we have discussed a homogeneous system. However, practically important materials are always inhomogeneous, and even for materials homogeneous in appearance, surfaces or interfaces lead to some inhomogeneity. As discussed in Sec. IV A, a metal surface is expected to have a smaller thermal diffusivity when it is observed in a mesoscopic length scale, even if the surface is a well-prepared ideal surface. Since the TRG signal we observed is closely concerned with heat diffusion in the mesoscopic length scale, we should introduce a depth-dependent thermal diffusivity $D(z)$. The problem is how to analyze a set of experimental data $S_{\mathrm{measured}}(t,\Lambda)$ to evaluate $D(z)$. In essence, this is a kind of inverse problem for which much research has been reported in the last decade for PT/PA techniques of nondestructive material evaluation.[29–31] The problem is solvable in principle, but there are many practical difficulties.

When we introduce $D(z)$ in Eq. (3), the corresponding solution of $u_Z(0,t)$ has an extremely complicated form and substantial time-consuming calculations are required for the solution. Therefore, it is indispensable to establish the simplest way to evaluate $D(z)$ with experimentally determined values. We start from Eq. (5c) for homogeneous materials to refine the relation between it and the empirical equation in Eq. (1). The form of Eq. (5c) implies that time-dependence of $u_Z(0,t)$ can be expressed as a convolution of three terms: a heat diffusion term,

$$\frac{\gamma_1}{\gamma_2(\gamma_1+\gamma_2)};$$

a thermal deformation term,

$$\frac{\gamma_1+\gamma_2+\gamma_3}{(\gamma_2+\gamma_3)(\gamma_3+\gamma_1)};$$

and a elastic deformation term,

$$\frac{\gamma_4^4-1}{(1+\gamma_4^2)^2-4\gamma_3\gamma_4}.$$

It should be noted that γ_1, γ_2, γ_3, and γ_4 represent optical, thermal, longitudinal acoustic, and shear acoustic contributions, respectively; the heat diffusion term has the same s-dependence as $\hat{\varphi}(0,s)$; the elastic deformation term has no influence from thermal properties; and the dispersion relation of SAW is given by $(1+\gamma_4^2)^2-4\gamma_3\gamma_4=0$.

We can consider that the surface-normal deformation $u_Z(0,t)$ is composed from two modes: one is the propagating SAW mode and the other is the nonpropagating thermal deformation mode. Such a mode separation of photothermal displacement has been reported on laser-induced bulk acoustic waves, and it provides a good approximation for a wide variety of materials at room temperature.[20] The idea of the mode separation gives some theoretical background for analysis using Eq. (1), in which time-dependent parts of thermal and acoustic contributions are given by $\exp(-t/\tau_T)$ and $\exp(-t/\tau_A)\cos\{2\pi F(t+t_D)\}$, respectively. Since the dispersion relation of SAW for a given wave number has only one single solution of real frequency value, the elastic deformation shows a monocyclic oscillation with time. By considering acoustic attenuation, the oscillation is expressed as $\exp(-t/\tau_A)\cos\{2\pi F(t+t_D)\}$. Since a smoothing operation can eliminate the oscillation, next we should consider the time-dependence, $\exp(-t/\tau_T)$.

If we neglect the elastic deformation term by replacing it with unity in Eq. (5c), we get a response, $u_{Z,\mathrm{thermal}}(0,t)$ by the thermal deformation mode. A calculated $u_{Z,\mathrm{thermal}}(0,t)$ for grating spacing of 2.5 μm is shown in Fig. 5(a). For comparison, $u_Z(0,t)$ and its smoothed response $u_{Z,\mathrm{smoothed}}(0,t)$ are also shown. The smoothing was performed in the same way as in analyzing the measured response described in Sec. II B. We can see the exponentially decaying feature of the u_Z response is owing to $u_{Z,\mathrm{thermal}}$. This is obvious when represented in a semilogarithmic plot in Fig. 5(b). As for the decay rate, it is clear that $u_{Z,\mathrm{smoothed}}$ is a good approximation for $u_{Z,\mathrm{thermal}}$. Further calculations confirm that the elastic property has almost no influence on the decay rate of $u_{Z,\mathrm{thermal}}$. Thus, we can expect to determine a decay rate τ_T for the thermal deformation mode from a measured response without substantial disturbances from elastic properties.

When heat diffusion is disturbed by inhomogeneity, the heat diffusion term should be modified, but the other terms are expected to experience little influence. If this is true, a good approximation for the thermally inhomogeneous system is to replace only the heat diffusion term by an appropriate form describing heat diffusion in the sample. Validity

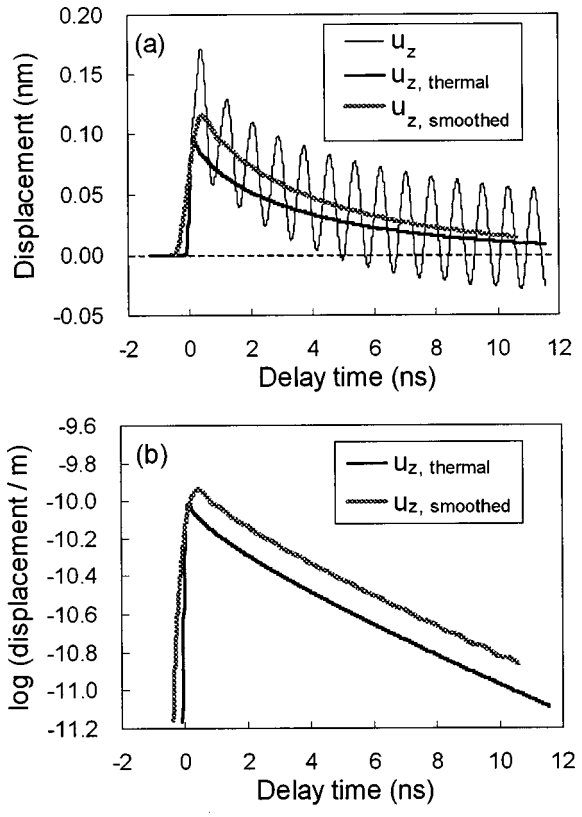

FIG. 5. Calculated responses of surface-parallel spatial modulation amplitudes in displacement to surface-normal direction plotted in (a) normal scale; and (b) semilogarithmic scale. The u_z represents both thermal and elastic contributions; $u_{z,\text{thermal}}$ is the thermal contribution only; and $u_{z,\text{smooth}}$ is a smoothed response of u_z. The grating spacing is 2.5 μm.

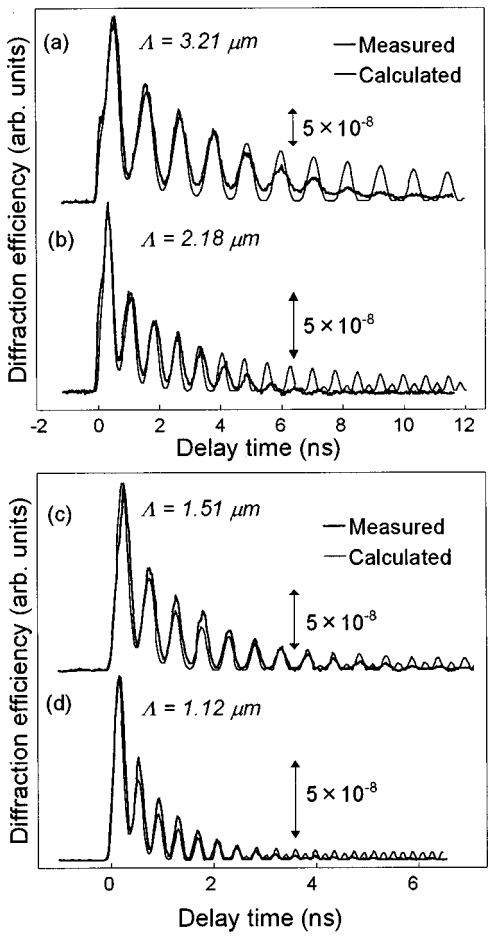

FIG. 6. TRG responses of the Ni single crystal at room temperature for grating spacings Λ of (a) 3.21 μm; (b) 2.18 μm; (c) 1.51 μm; and (d) 1.12 μm. All traces are normalized to a unit height, and calculated diffraction efficiency is shown as double-ended arrows. Measured and calculated responses are shown for each grating spacing for comparison. Their discrepancy is larger as grating spacing becomes smaller.

of the approximation should be tested for various types of $D(z)$ distributions. However, it seems valid for the Ni crystal where the response by the heat diffusion term is much slower than responses by the deformation terms, even by the slowest contribution from SAW.

We think of a further approximation in which only the heat diffusion term is used to calculate τ_T. We confirmed that calculations ignoring the two deformation terms in Eq. (5c) systematically generated ca. 13% smaller $1/\tau_T$ for the case of a uniform thermal property. The most important point is this approximation strongly simplifies analysis of a thermally inhomogeneous system. Thus, the present depth profiling analysis is based on this approximation. As one of the simplest cases of the $D(z)$ distribution, we adopt the two-layer model where a layer with a finite thickness L is on a semi-infinite bulk substance. The sample is assumed to have thermal diffusivities of D_1 for the layer and D_2 for the substrate. By assuming the density, heat capacity, and optical absorption coefficient have no depth-dependent variation, we can calculate TRG responses only from the heat diffusion term. After that, τ_T is calculated in the same manner as for experimental data. To get a depth profile, a set of experimental $\tau_T(\Lambda)$ is compared with a calculated set, where L and D_1 are adjusted to minimize the summation of squared errors between the data sets. For D_2, we use a reference value. The results are discussed in Sec. IV C.

IV. RESULTS AND DISCUSSION

A. TRG responses of the Ni single crystal

Both experimental and theoretically calculated TRG responses of the Ni single crystal are shown in Figs. 6 and 7. In each figure, four sets of measured and calculated traces are presented where each set corresponds to different measurement conditions. The calculated traces are obtained as described in Secs. III A and III B with materials properties obtained from the literature.[32,33] Each trace is normalized to a fixed height and numerical values by double-ended arrows in these figures indicate theoretically estimated diffraction efficiency.[13]

In Fig. 6, grating spacings are varied from 1.1–3.2 μm at room temperature. For each grating spacing, the measured and calculated results have a similar shape. Since we neglect acoustic attenuation in the theoretical calculation, it is reasonably understood that acoustic dumping is weaker for the theoretical curves than the measured curves. We find that the intensity ratios among first, second, and third peaks show better agreement when the grating spacing is larger. A deviation is apparent for data of 1.12 μm grating spacing.

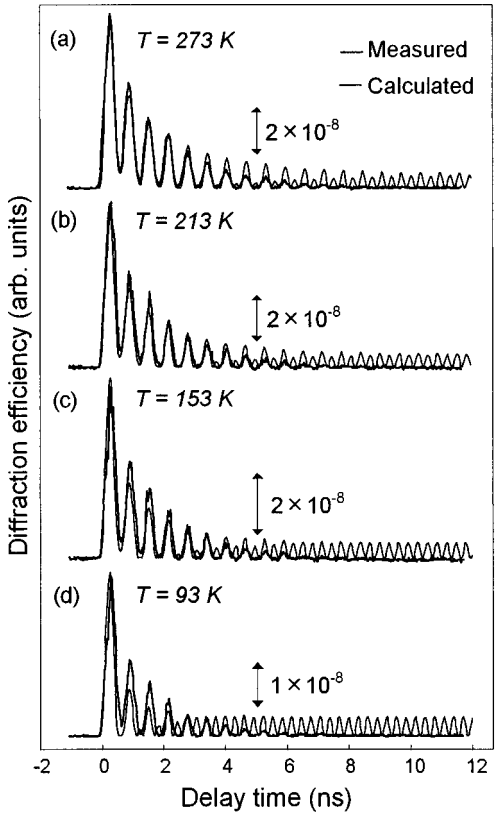

FIG. 7. TRG responses of the Ni single crystal for sample temperature T of (a) 273 K; (b) 213 K; (c) 153 K; and (d) 93 K. The grating spacing is 1.84 μm. All traces are normalized to a unit height, and calculated diffraction efficiency is shown as double-ended arrows. Measured and calculated responses are shown for each temperature. Their discrepancy is larger as temperature becomes lower.

Traces in Fig. 7 are obtained when the sample temperature is set at four different values between 93–273 K while the grating spacing is kept at 1.84 μm. Roughly, the measured and calculated results have a similar shape for each sample temperature. Discrepancies between measured and calculated data at a larger delay time are due to our neglecting acoustic attenuation in the calculation. In addition to those points, we find deviations are more enhanced at lower temperature as is apparent from the initial part of traces (c) and (d) in Fig. 7.

Theoretically-calculated and experimentally-measured data show better agreement when measurements are done with larger grating spacings and at room temperature. We think deviations at low temperature or small grating spacing come from the same physical origin. Decrease in thermal diffusivity at a near-surface region is the most probable candidate. The fact that measured responses decrease more slowly with time than calculated responses corresponds to a smaller thermal diffusivity of the measured sample than the reference value used in the calculation. The observed deviation is probably caused by some surface effects because a smaller grating spacing results in a larger deviation.

We can easily expect an intrinsic surface effect of thermal diffusivity although there are no reports in the literature to our knowledge that directly describe it. Heat conduction in metal is mainly dominated by free electrons. Thermal conductivity κ and electrical conductivity σ are described in a linear relationship known as the Wiedemann-Franz law.[5] On the other hand, a metal surface exhibits specific electrical conductivity due to electron scattering by the surface. When the diameter d of a metallic sample is reduced to the size of the mean-free-path of electrons in the bulk metal l_B, then the electrical conductivity of the metal is found to decrease below its value for bulk metal σ_B. The equation for such a decrease is derived from kinetic theory arguments and given by an approximation formula[4]

$$\sigma = \sigma_B / [1 + (l_B/d)(1-p)/(1+p)], \tag{8}$$

where p is a fraction of the electrons scattered specularly, i.e., conserving the component of crystal momentum parallel to the scattering surface. As in most cases in measuring size-effects of conductivity, completely diffuse scattering ($p = 0$) is assumed. For Ni, l_B/σ_B at 300 K are reported[33] as 3.5, 3.8, and 3.7×10^{-11} Ω cm^2. These values correspond to l_B of 57, 61, and 60 nm for $1/\sigma_B$ of 6.2 $\mu\Omega$ cm.[4]

These lengths could cause substantial effects for our present observation. As mentioned in Sec. II thermal observation depth is varied with the grating spacings. Typical observation depths are 170–570 nm, corresponding to grating spacings of 1.05–3.59 μm used in this study. The shortest one is only three times larger than the electron mean-free-path in Ni at 300 K. Since the electron mean-free-path is longer at lower temperature, we can expect an increase in the contribution of the surface effect to heat conductivity at lower temperatures.

B. Temperature dependencies of thermal diffusivity and SAW velocity

Next we present details of the analysis of the decrease in thermal diffusivity at the Ni surface. From a set of TRG responses measured with a grating spacing of 1.84 μm and during temperature control, we deduced temperature dependencies of thermal diffusivity D_{eff} and SAW velocity V_{SAW}. The results are shown in Fig. 8. Error bars in Fig. 8 indicate the standard deviations. Since the observation depths are 290 nm for the thermal diffusivity and 920 nm for SAW velocity corresponding to the grating spacing of 1.84 μm, measured data are referred to as surface values. On the other hand, smooth curves are referred to as bulk values because they are interpolated using literature values for bulk crystals of Ni.[32]

There is no reduction in SAW velocity showing acoustic phonons are important for reduction in thermal diffusivity. At a lower temperature, a substantial decrease in thermal diffusivity, which is overestimated as discussed in Sec. II C is obvious. Some parts of the decrease may be due to restriction of electron mean-free-path by the surface itself, but it seems the decrease is much larger at a low temperature than that expected from only the restriction.

C. Depth profiling analysis of thermal diffusivity $D(z)$

To quantitatively analyze the surface effects, we performed a depth profiling analysis of thermal diffusivity. We corrected TRG responses at room temperature for a set of grating spacings and calculated a decay rate of $1/\tau_T$ for each response. The results are summarized in Fig. 9. Observation

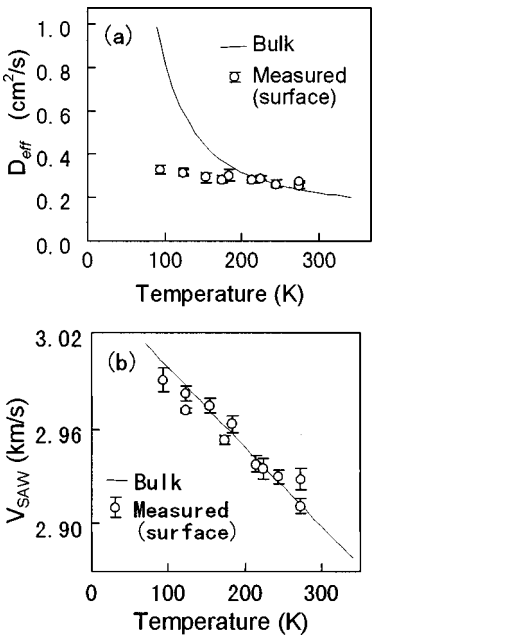

FIG. 8. Temperature dependence of (a) thermal diffusivity D_{eff} and (b) surface acoustic wave velocity V_{SAW} for the Ni single crystal. Grating spacing is 1.84 μm corresponding to the observation depth of 290 nm. Open circles and error bars represent averaged values determined by TRG measurements and their standard deviations, respectively. Smoothed curves are calculated by interpolating literature values.

depth is indicated on the upper horizontal axis. This figure shows the depth profile of the diffusivity because $1/\tau_T$ is a function of thermal diffusivity. Shaded circles and error bars attached to them are the averaged values and the standard deviations, respectively. Two smoothed curves in Fig. 9 are theoretically calculated based on two different models.

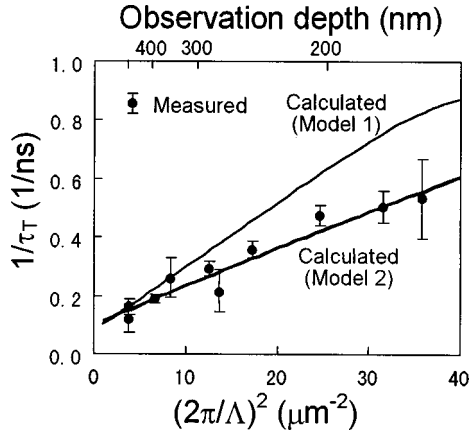

FIG. 9. Grating spacing (Λ) dependence of thermal relaxation rate ($1/\tau_T$) of the Ni single crystal. Observation depth corresponding to a grating spacing is shown on the upper axis. Shaded circles and error bars represent averaged values determined by TRG measurements and their standard deviations, respectively. Smoothed curves are theoretically calculated for two models. Model 1 assumes a uniform distribution of thermal diffusivity of 0.22 cm^2/s. Model 2 assumes one layer with thickness of 270 nm and thermal diffusivity of 0.11 cm^2/s over a substrate with infinite thickness and thermal diffusivity of 0.22 cm^2/s.

Model 1 assumes a homogeneous distribution of thermal diffusivity whose magnitude is the same as the literature value, 0.22 cm^2/s. Shown as the thin line in Fig. 9, this model fails to express the experimental data well. Considering the approximation we used, the discrepancy between the model 1 prediction and the experimental data is much larger. If we ignore that, we need to assume a thermal diffusivity of 0.14 cm^2/s to get good agreement for the uniform model. This value is 36% smaller than the literature value and is outside the order for the Ni crystal.

Even if we take a photo-induced temperature increase at the surface into account, we cannot explain the experimental data. Maximum value of the temperature increase just after pump laser irradiation is less than 50 K at the interference maxima as shown in Fig. 4(a). The 50 K temperature rise from 300 K makes less than a 12% decrease in thermal diffusivity. The experimental data require much lower thermal diffusivity.

In model 2, we assume a material system consisted of one layer with a finite thickness existing on an infinite substrate where thermal diffusivities of the layer and substrate are different. The substrate is assumed to have the same magnitude of thermal diffusivity as the literature value, 0.22 cm^2/s. We optimize thickness and thermal diffusivity of the upper layer to minimize the summation of the squared errors. As the best fitting result, 0.11 cm^2/s thermal diffusivity and 270 nm layer thickness are obtained. Calculated values of $1/\tau_T$ with these values are plotted as the thick line in Fig. 9. The theoretical curve of model 2 agrees well with experimental data. The thickness 270 nm is 4.5 times larger than the electron mean-free-path. Electron scattering by the surface can explain only a portion of the decrease, 18% $[=1-1/(1+60/270)]$. We think there must be lattice disorders in the mesoscopic subsurface region, which seem to be introduced during cutting of the crystal or polishing its surface.

When we compare the results of model 2 with those of model 1 with 0.14 cm^2/s thermal diffusivity, it is difficult to decide which is better only from magnitudes of the summation of the squared errors. The magnitude is slightly smaller for model 2, but the approximation used here is too rough for a final judgment. We often met such a kind of problem when carrying out depth profiling. For an inverse problem like this, it seems essential to get some additional information such as thermal diffusivity of the bulk, with which we can make a judgment.

This is a first example of sub-μm level depth profiling of a thermal property. Evaluation and control of the thermal property for mesoscopic size will be important in fabrication of micromachines and large-scale integrated circuits of next generation.

V. CONCLUSION

TRG responses can reflect slight changes in interactions at a surface and interface. We have measured and theoretically calculated TRG responses for a Ni single crystal under temperature control from 80–293 K and with a variety of grating spacings from 1–4 μm. Comparing results, we found larger grating spacing and higher sample temperature provided better agreement. Deviations between them at lower temperature or smaller grating spacings were attributed to a decrease

of thermal diffusivity at the sample surface. By introducing a simplified method for calculating the thermal relaxation rate constant $1/\tau_T$ for inhomogeneous materials, we demonstrated sub-μm level depth profiling of thermal diffusivity. Surface properties are not the same as bulk properties. For thermal properties, a mesoscopic size of less than sub-μm is crucial. This level of size will be coming into the realm of investigation. It seems important to measure and determine characteristic surface properties for practical materials since real surfaces experience unexpected influences due to surface preparation procedures. For fast heat transport from solid to liquid, some recent experiments[11] have suggested a contribution from atomic scale thermal barriers, which are caused by adsorption of molecules at the interface. Mesoscopic observations proceeding from macroscopic ones will help us to link a microscopic understanding of heat transport when aided by molecular dynamic simulations or computational calculations.

[1] *8th International Topical Meeting on Photoacoustic and Photothermal Phenomena*, edited by D. Fournier and J. P. Roger [J. Phys. IV, **C7** (1994)].

[2] *9th International Topical Meeting on Photoacoustic and Photothermal Phenomena*, edited by S.-Y. Zhang [Prog. Nat. Sci., Suppl. **6** (1996)].

[3] A. Harata and T. Sawada, Trends Anal. Chem. **14**, 504 (1995).

[4] J. Boss in *Landolt-Börnstein Numerical Data and Functional Relationships in Science and Technology*, edited by O. Madelung, Landolt-Börnstein, New Series, Group III, Vol. 15, Part 1a (Springer-Verlag, Berlin, 1982), p. 141.

[5] C. Kittel, *Introduction to Solid State Physics*, 5th ed. (Wiley, New York, 1976).

[6] S. Kimura, J. Mizuki, J. Matsui, T. Ishikawa, and T. Ishikawa, Appl. Phys. Lett. **60**, 2604 (1992).

[7] H. J. Eichler, P. Gunter, and D. W. Pohl, *Laser-Induced Dynamic Gratings*, edited by T. Tamir (Springer-Verlag, Berlin, 1986) Vol. 50, Chap. 1, p. 1.

[8] A. Harata, H. Nishimura, and T. Sawada, Appl. Phys. Lett. **57**, 132 (1990).

[9] I. M. Fishman, C. D. Marshall, A. Tokmakoff, and M. D. Fayer, J. Opt. Soc. Am. B **10**, 1006 (1993).

[10] A. Harata and T. Sawada, Appl. Phys. Lett. **58**, 1839 (1991).

[11] A. Harata, T. Kawasaki, M. Ito, and T. Sawada, Anal. Chim. Acta **299**, 349 (1995).

[12] A. R. Duggal, J. A. Rogers, and K. A. Nelson, J. Appl. Phys. **72**, 2823 (1992).

[13] A. Harata, Q. Shen, T. Tanaka, and T. Sawada, Jpn. J. Appl. Phys., Part 1 **32**, 3633 (1993).

[14] A. Harata, Q. Shen, T. Tanaka, and T. Sawada, in *8th International Topical Meeting on Photoacoustic and Photothermal Phenomena*, edited by D. Fournier and J. P. Roger [J. Phys. IV **C7**, 159 (1994)].

[15] O. W. Käding, M. Rösler, R. Zachai, H.-J. Füßer, and E. Matthias, Diamond Relat. Mater. **3**, 1178 (1994).

[16] G. W. Farnell, *Acoustic Surface Waves*, edited by A. A. Oliner (Springer-Verlag, Berlin, 1978).

[17] R. J. D. Miller, *Time-Resolved Spectroscopy*, edited by R. J. H. Clark and R. E. Hester (Wiley, Chichester, 1989) p. 1.

[18] S. M. Gracewski and R. J. D. Miller, J. Chem. Phys. **103**, 1191 (1995).

[19] Q. Shen, A. Harata, and T. Sawada, Jpn. J. Appl. Phys., Part 1 **35**, 2339 (1996).

[20] F. A. McDonald and G. C. Wetsel, Jr., *Physical Acoustics*, edited by W. P. Mason and R. N. Thurston (Academic, San Diego, 1986), Vol. 18, p. 186.

[21] M. Born and E. Wolf, *Principle of Optics*, 5th ed. (Pergamon, Oxford, 1975).

[22] M. Aeschimann, M. Bauer, and S. Pawlik, Chem. Phys. **205**, 127 (1996).

[23] T. Hosono, Radio Sci. **16**, 1015 (1981).

[24] T. Hosono, *Fast Laplace Transform by BASIC* (Kyouritu, Tokyo, 1984) in Japanese.

[25] V. I. Krylov and N. S. Skoblya, *Handbook of Numerical Inversion of Laplace Transforms* (IPST, Jerusalem, 1969).

[26] K. J. Faran, R. J. D. Miller, and S. M. Gracewski, J. Appl. Mech. **57**, 415 (1990).

[27] *Handbook of Optical Constants of Solids*, edited by E. D. Palik (Academic, Orlando, 1985).

[28] K. Katayama, Q. Shen, A. Harata, and T. Sawada, Appl. Phys. Lett. **69**, 17 (1996).

[29] A. Harata and T. Sawada, J. Appl. Phys. **65**, 959 (1989).

[30] A. Mandelis, S. B. Peralta, and J. Thoen, J. Appl. Phys. **70**, 1761 (1991).

[31] T.-C. Ma, M. Munidasa, and A. Mandelis, J. Appl. Phys. **71**, 6029 (1992).

[32] *American Institute of Physics Handbook*, 3rd ed., edited by D. E. Gray (McGraw-Hill, New York, 1972).

[33] *Landolt-Börnstein Numerical Data and Functional Relationships in Science and Technology* (Ref. 4), p. 5.